

PAPER • OPEN ACCESS

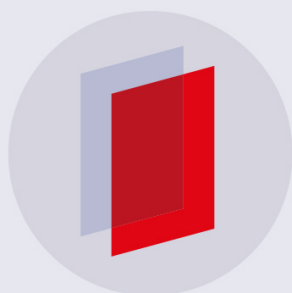
## Robust quantum spin Hall state and quantum anomalous Hall state in graphenelike $\text{BC}_3$ with adatoms

To cite this article: Yinchang Zhao *et al* 2018 *New J. Phys.* **20** 073047

View the [article online](#) for updates and enhancements.

### Related content

- [Quantum anomalous Hall effect in real materials](#)  
Jiayong Zhang, Bao Zhao, Tong Zhou et al.
- [Giant gap quantum spin Hall effect and valley-polarized quantum anomalous Hall effect in cyanided bismuth bilayers](#)  
Wei-xiao Ji, Chang-wen Zhang, Meng Ding et al.
- [Quantum anomalous Hall effect and topological phase transition in two-dimensional antiferromagnetic Chern insulator  \$\text{NiOsCl}\_6\$](#)   
Wei-Wei Yang, Lei Li, Jing-Sheng Zhao et al.



**IOP | ebooks**<sup>TM</sup>

Bringing you innovative digital publishing with leading voices to create your essential collection of books in STEM research.

Start exploring the collection - download the first chapter of every title for free.



## PAPER

Robust quantum spin Hall state and quantum anomalous Hall state in graphenelike  $BC_3$  with adatoms

## OPEN ACCESS

## RECEIVED

30 May 2018

## REVISED

6 July 2018

## ACCEPTED FOR PUBLICATION

13 July 2018

## PUBLISHED

26 July 2018

Original content from this work may be used under the terms of the [Creative Commons Attribution 3.0 licence](https://creativecommons.org/licenses/by/4.0/).

Any further distribution of this work must maintain attribution to the author(s) and the title of the work, journal citation and DOI.

Yinchang Zhao<sup>1,5</sup>, Xi Chen<sup>2</sup>, Zhenhong Dai<sup>1,5</sup> , Chao Zhang<sup>1</sup> , Chao Lian<sup>3</sup>, Shuming Zeng<sup>2</sup>, Sheng Meng<sup>3,4,5</sup> and Jun Ni<sup>2,4,5</sup><sup>1</sup> Department of Physics, Yantai University, Yantai 264005, People's Republic of China<sup>2</sup> State Key Laboratory of Low-Dimensional Quantum Physics, Department of Physics, Tsinghua University, Beijing 100084, People's Republic of China<sup>3</sup> Beijing National Laboratory for Condensed Matter Physics and Institute of Physics, Chinese Academy of Sciences, Beijing, 100190, People's Republic of China<sup>4</sup> Collaborative Innovation Center of Quantum Matter, Beijing 100084, People's Republic of China<sup>5</sup> Authors to whom any correspondence should be addressed.E-mail: [y.zhao@ytu.edu.cn](mailto:y.zhao@ytu.edu.cn), [zh dai@ytu.edu.cn](mailto:zh dai@ytu.edu.cn), [smeng@iphy.ac.cn](mailto:smeng@iphy.ac.cn) and [junni@mail.tsinghua.edu.cn](mailto:junni@mail.tsinghua.edu.cn)

Keywords: quantum spin Hall effect, quantum anomalous Hall effect, topological insulator, Chern insulator

## Abstract

Two-dimensional (2D) topological insulators (TIs) and Chern insulators (CIs) promise quantum spin Hall (QSH) and quantum anomalous Hall (QAH) states without dissipation. By combining first-principles calculations with Wannier functions-based tight-binding (TB) modeling, we demonstrate that the graphenelike  $BC_3$ , which was fabricated early in experiment, can become 2D TIs and CIs through suitable decoration of adatoms. For the thallium (Tl) decorated  $BC_3$  systems, three low-energy structures with the same stoichiometry of  $BC_3Tl$ , whose stabilities are verified by the *ab initio* evolutionary algorithm, are found to be robust 2D TIs with the largest topologically nontrivial band gap of about 224 meV. For the transition metal atoms adsorbed  $BC_3$ , three ( $2 \times 2$ )  $BC_3$  systems with one adatom of technetium (Tc), rhenium (Re), or ruthenium (Ru) are found to be good CIs with the ferromagnetic moments of 1 to  $2 \mu_B$ , nontrivial gaps of 38–50 meV, and nonzero Chern numbers of  $-1$  to 1. These properties indicate that the systems of graphenelike  $BC_3$  with adatoms are good platforms for the study of QSH and QAH effects.

## 1. Introduction

Topological insulators (TIs), characterized by insulating bulk and metallic surface or edge states, have attracted great interest [1–3]. The carriers in the surface or edge states of TIs are helical Dirac fermions behaving as massless relativistic particles with an intrinsic spin locked to its translational momentum due to time-reversal symmetry (TRS) [4], which allows a possible realization of dissipationless coherent spin transport [5, 6]. Specially, in two-dimensional (2D) TIs (also known as quantum spin Hall (QSH) insulators), the carriers in the edge states only move along two directions with opposite spins, and thus are insensitive to nonmagnetic edge modification, making the 2D TIs be more suitable for dissipationless device applications [7]. Unfortunately, it is challengeable to realize 2D TIs experimentally, although many three-dimensional TIs are identified [8, 9]. To date, only the HgTe/CdTe and InAs/GaSb/AlSb quantum well systems are well-established, but their bulk gaps are too small, with the QSH effect observed only below 10 K [10–12]. Hence hunting of feasible room-temperature QSH insulators is of great significance for practical applications. To this end, extensive effort has been devoted and many strategies to obtain the 2D TIs with large nontrivial gaps have been followed [13–18].

Chern insulators (CIs), also called quantum anomalous Hall (QAH) insulators, are 2D magnetic insulators showing quantized anomalous Hall conductivities  $Ce^2/h$  with  $C$  as an integer topological index (the so-called Chern number) [19]. The essential ingredients of CIs are the spontaneous TRS breaking and the presence of spin-orbit coupling (SOC), which gives rise to a net Berry curvature needed for the nonzero Chern number. So far, a number of theoretical proposals have been made to realize the CIs states [20–26]. The typical examples are the magnetically

doped TIs [20, 21], which results in the first experimental observation of QAH effects in Cr doped (Bi, Sb)<sub>2</sub>Te<sub>3</sub> films [27], a milestone discovery in search of novel topological states. Besides the magnetically doped TIs, many honeycomb or square lattices composed of transition metal and heavy-metal ions have been also proposed to be potential CIs [22–26]. For instance, a hexagonal lattice formed by molecular building blocks of triphenyl-transition metal compounds has been confirmed to be a class of organic CIs with nonzero Chern numbers and nontrivial band gaps [23]; a square CrO<sub>2</sub>/TiO<sub>2</sub> superlattice has been reported to be a CI with a Chern number of  $\pm 2$  [26], etc.

Recently, atom adsorbed or functionalized graphene, silicene, germanene, and stanene have been proposed to be potential 2D TIs and CIs [13, 14, 22, 28, 29]. However, in graphene adsorption systems, the adatoms are weakly adsorbed on graphene, and the nontrivial gaps opened are usually small and far away from Fermi level [30]. In silicene, germanene, and stanene based systems, the binding between adatoms and substrates is much enhanced, and the nontrivial gaps are also enlarged due to the enhancement of SOC. But the facts that silicene, germanene, and stanene have inferior mechanical strength than graphene and cannot be produced by micromechanical exfoliation put forward new challenges in experiments to realize QSH and QAH states in these materials based systems. Therefore, a new system based on a 2D material as stable as graphene is required for seeking robust QSH and QAH states. Here we turn to the graphenelike BC<sub>3</sub> to seek these novel topological states.

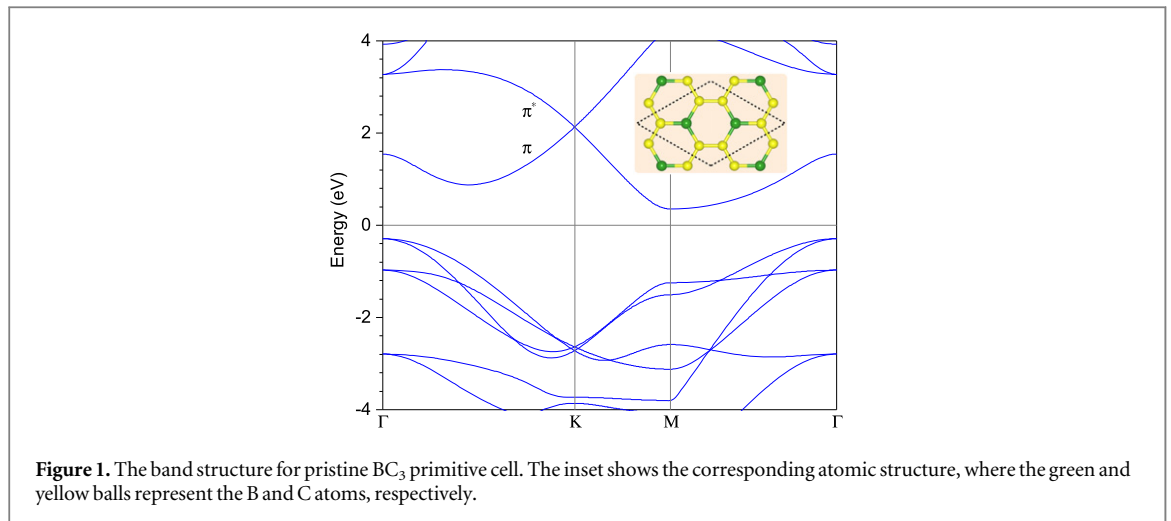
The graphenelike BC<sub>3</sub>, which has been fabricated in experiment [31], has mechanical strength comparable to graphene. The binding between adatoms and BC<sub>3</sub> is also much enhanced relative to that in graphene adsorption systems [32–34]. Moreover, the bulk BC<sub>3</sub> produced early by chemical synthesis is formed by stacked layers that are coupled by Van der Waals interaction [35], which makes the fabrication of BC<sub>3</sub> sheet be probable by micromechanical exfoliation from the bulk counterpart, same as the production of graphene from graphite [36]. To date, high-capacity hydrogen storage [32, 33], tunable Fermi surface nesting-derived magnetic phase [34], and novel topological  $p + ip$  superconductivity [37] have been studied in BC<sub>3</sub> based systems. But the topological properties of this 2D material is lacking. In this paper, we systematically study the topological electronic properties of BC<sub>3</sub>, and demonstrate that it can become 2D TIs and CIs through suitable decoration of adatoms. We find that three structures of thallium (Tl) decorated BC<sub>3</sub> are robust 2D TIs with the largest nontrivial gap of 224 meV, and three kinds of transition metal atoms adsorbed BC<sub>3</sub> are good CIs with the nonzero Chern numbers and nontrivial gaps exceeding 38 meV. These findings indicate that the systems of graphenelike BC<sub>3</sub> with adatoms are good platforms for realizing QSH and QAH effects.

## 2. Methodology

Our first-principles calculations are carried out within the density functional theory implemented in VASP [38, 39]. The projector augmented wave potentials [40] and a plane-wave basis set with the cutoff energy of 520 eV and the exchange–correlation functional of generalized gradient approximation (GGA) of Perdew–Burke–Ernzerhof (PBE) [41] are utilized to model the ion cores and valence electrons, respectively. A vacuum space larger than 18 Å is taken to eliminate the interaction between adatom–BC<sub>3</sub> layer and its periodic images. The atomic geometries are fully relaxed until the Hellman–Feynman force on each atom is less than 0.01 eV Å<sup>-1</sup>. For the adsorption systems within (1 × 1), (1 ×  $\sqrt{3}$ ), ( $\sqrt{3}$  ×  $\sqrt{3}$ ), and (2 × 2) BC<sub>3</sub> supercells, the  $\Gamma$ -centered Monkhorst–Pack sampling grid of 18 × 18 × 2, 18 × 12 × 2, 12 × 12 × 2, and 9 × 9 × 2 are used to simulate their electron-momentum integrations, respectively. To gain stable adsorption structures, the total energies of all possible adsorption configurations are traversed. After the energetically stable structures are confirmed, the required tight-binding (TB) models in calculations of topological properties are created from maximally localized Wannier functions (MLWF) via Wannier90 package [42]. Based on the MLWF TB models, the topological electronic properties are calculated by Wannier Tools [43]. These calculations are checked by Z2Pack program [44] and *postw90.x* code of Wannier90 package [42], and consistent results are obtained. In addition, for further verifying the energy stabilities of the Tl decorated BC<sub>3</sub> systems, the structure searches based on *ab initio* evolutionary algorithm coded in USPEX [45–47] are also performed with the low-energy structures obtained from traversal as input seeds.

## 3. Results and discussion

Due to the lack of dangling bonds, the graphenelike BC<sub>3</sub>, which has eight atoms in each primitive cell and shares the same point group with graphene, is a semiconductor with an indirect band gap of 0.62 eV, as shown in figure 1. The first and second conduction bands are the  $\pi$  and  $\pi^*$  bands, respectively. At the K (K') point, there is a Dirac cone with the degeneracy between the  $\pi$  and  $\pi^*$  bands. Because of the composition of light elements, the intrinsic SOC of BC<sub>3</sub> is very weak, which makes the SOC gap opened at the Dirac cone be fairly small, similar to that in graphene [28]. Hence it is essential to adsorb metal atoms to enhance SOC, and the adsorbed metal atoms should contain valence electrons of  $p$  or  $d$  orbitals because the electrons of these orbitals have nonzero SOC according to  $\hat{H}_{\text{SOC}} = \lambda \hat{L} \cdot \hat{S} = \frac{\lambda}{2} [\hat{J}^2 - \hat{L}^2 - \hat{S}^2]$  with  $\hat{J} = \hat{L} + \hat{S}$ . Meanwhile, the decoration of metal



adatoms must provide electron doping to  $BC_3$ , giving rise to the shift of Fermi level towards Dirac cone. In addition, the binding between adatoms and  $BC_3$  should be as strong as possible to form stable adsorption.

### 3.1. QSH states in TI decorated $BC_3$ sheets

Based on the requirements above, we find that suitable adsorption of TI atoms on  $BC_3$  maintains the Dirac cone character and shifts Fermi level just to the Dirac cone simultaneously. These adsorption systems are the configurations with the stoichiometry of  $BC_3TI$ , which corresponds to each  $BC_3$  primitive cell adsorbing with two TI atoms. Via traversing the total energies of all possible adsorption configurations for the  $(1 \times 1)$ ,  $(1 \times \sqrt{3})$ ,  $(\sqrt{3} \times \sqrt{3})$ , and  $(2 \times 2)$   $BC_3$  supercells, we obtain four low-energy structures, as shown in figures 2(a)–(d), in which TI atoms tend to be adsorbed uniformly on each side of  $BC_3$  sheet and fall on the hollow site of the  $B_2C_4$  rings of  $BC_3$ . According to their space groups and sizes of the  $BC_3$  supercells, the four low-energy structures are designated as  $C222@(1 \times 1)$ ,  $Pmna@(1 \times \sqrt{3})$ ,  $Pma2@(1 \times \sqrt{3})$ , and  $P-3m1@(\sqrt{3} \times \sqrt{3})$ , as shown in figures 2(a)–(d), respectively. The binding energies between adatoms TI and  $BC_3$  in these structures are calculated by  $E_b = E_{BC_3} + E_{TI} - E_{BC_3TI}$ , where  $E_{BC_3}$ ,  $E_{TI}$ , and  $E_{BC_3TI}$  are the total energies of bare  $BC_3$  sheet, isolated TI atom, and adsorption system, respectively. The calculated binding energies  $E_b$  together with the structural parameters of these structures are listed in table 1. The values of  $E_b$  exceed the calculated cohesive energy  $E_c$  ( $\sim 1.95$  eV) of the bulk TI metal, which means that the clustering of adatoms TI is completely suppressed.

The four low-energy adsorption structures can be taken as stable monolayer  $BC_3TI$  films with a fixed thickness of 2.35 Å, as listed in table 1. To verify whether these structures are more stable than other possible  $BC_3TI$  films, we search more 2D  $BC_3TI$  allotropes based on *ab initio* evolutionary algorithm. The searches are performed in the unit cells containing  $n$  units of  $BC_3TI$ , where the integer  $n = 2, 3, 4, 5, 6, 7$ , and 8, which means that there are 10, 15, 20, 25, 30, 35, and 40 atoms, respectively, in the unit cells for each search. The initial structures are randomly generated using the plane group symmetry with a given initial thickness of 4.5 Å. In the searches with the unit cells containing 10, 20, and 30 atoms, the structures of  $C222@(1 \times 1)$ ,  $Pmna/Pma2@(1 \times \sqrt{3})$ , and  $P-3m1@(\sqrt{3} \times \sqrt{3})$  are taken as their respective input seeds. Our search findings indicate that the structures with lower total enthalpies are found in the unit cells containing 10, 20, and 30 atoms. In all of the newly found  $BC_3TI$  allotropes, only the four seed configurations of  $C222@(1 \times 1)$ ,  $Pmna@(1 \times \sqrt{3})$ ,  $Pma2@(1 \times \sqrt{3})$ , and  $P-3m1@(\sqrt{3} \times \sqrt{3})$  are the energetically stable structures, as shown in figures 2(e)–(g). Moreover, the phonon dispersion calculations demonstrate that all of these four structures locate at the local minimums in the energy landscapes due to the absence of any imaginary frequency in the phonon dispersion spectra, as shown in figure A1 in the appendix. These results imply that the four stable  $BC_3TI$  adsorption structures may be synthesized directly on a suitable substrate in an epitaxial way.

The band structures excluding and including SOC for the four stable  $BC_3TI$  structures based on the GGA-PBE calculations are plotted in the left and middle panels in figure 3. When the SOC is excluded, these structures are semimetals with Fermi level just at the Dirac cone. The atomic orbital projections on the bands exhibit that a fairly large part of the Dirac cone states are contributed by the  $p$  orbital electrons of the adatoms TI, which hints strong SOC in these systems. As a result, when the SOC is included, the Dirac cones are prominently split, as shown in the middle panels in figure 3, and thus the large opened band gaps of 224, 220, and 200 meV are obtained for the  $C222@(1 \times 1)$ ,  $Pmna@(1 \times \sqrt{3})$ , and  $Pma2@(1 \times \sqrt{3})$  structures, respectively, as listed in table 1. However, the opened gap for the  $P-3m1@(\sqrt{3} \times \sqrt{3})$  structure is only 20 meV, which will be interpreted later. Due to three of the four stable  $BC_3TI$  structures being noncentrosymmetric, the  $\mathbb{Z}_2$  invariants

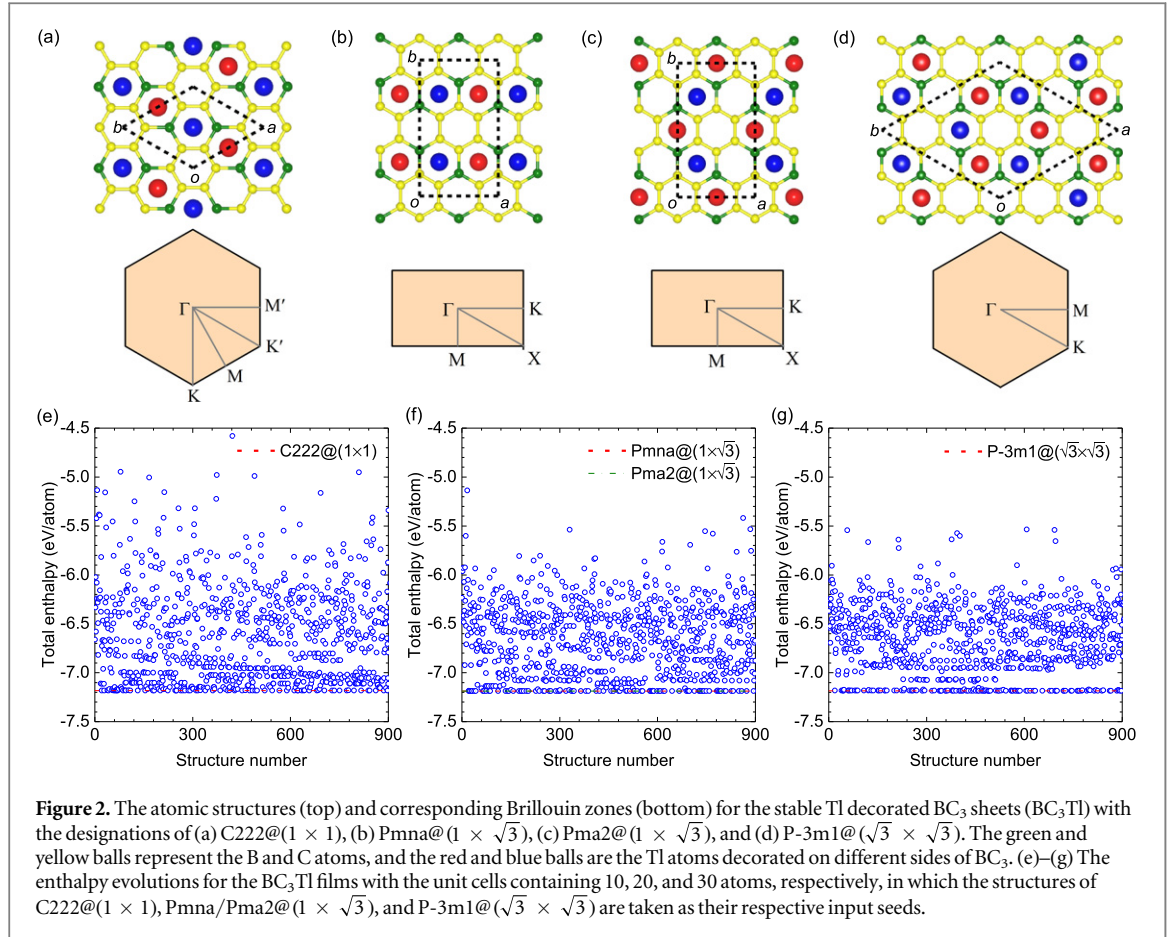


**Figure 2.** The atomic structures (top) and corresponding Brillouin zones (bottom) for the stable TI decorated  $BC_3$  sheets ( $BC_3TI$ ) with the designations of (a)  $C222@(1 \times 1)$ , (b)  $Pmna@(1 \times \sqrt{3})$ , (c)  $Pma2@(1 \times \sqrt{3})$ , and (d)  $P-3m1@(\sqrt{3} \times \sqrt{3})$ . The green and yellow balls represent the B and C atoms, and the red and blue balls are the TI atoms decorated on different sides of  $BC_3$ . (e)–(g) The enthalpy evolutions for the  $BC_3TI$  films with the unit cells containing 10, 20, and 30 atoms, respectively, in which the structures of  $C222@(1 \times 1)$ ,  $Pmna/Pma2@(1 \times \sqrt{3})$ , and  $P-3m1@(\sqrt{3} \times \sqrt{3})$  are taken as their respective input seeds.

**Table 1.** The calculated structural parameters (lattice vectors  $a$  and  $b$ , included angle  $\gamma$  between  $a$  and  $b$ , and thickness  $\delta$ ), binding energies ( $E_b$ ) between adatoms TI and  $BC_3$  sheet, ratios between  $E_b$  and cohesive energy  $E_c$  ( $\sim 1.95$  eV) of bulk TI metal ( $E_b/E_c$ ), nontrivial band gaps ( $E_g$ ), and  $\mathbb{Z}_2$  invariants for the TI decorated  $BC_3$  sheets ( $BC_3TI$ ) with the designations of  $C222@(1 \times 1)$ ,  $Pmna@(1 \times \sqrt{3})$ ,  $Pma2@(1 \times \sqrt{3})$ , and  $P-3m1@(\sqrt{3} \times \sqrt{3})$ .

$BC_3TI$	$a$ (Å)	$b$ (Å)	$\gamma$ (°)	$\delta$ (Å)	$E_b$ (eV)	$E_b/E_c$	$E_g$ (meV)	$\mathbb{Z}_2$
$C222@(1 \times 1)$	5.21	5.22	120.05	2.35	2.07	1.06	224	1
$Pmna@(1 \times \sqrt{3})$	5.21	9.02	90	2.35	2.07	1.06	220	1
$Pma2@(1 \times \sqrt{3})$	5.21	9.02	90	2.35	2.07	1.06	200	1
$P-3m1@(\sqrt{3} \times \sqrt{3})$	9.03	9.03	120	2.35	2.07	1.06	20	1

of these structures are calculated by the evolution of Wannier charge centers during the time-reversal pumping process, which is a method independent of the presence of inversion symmetry [48, 49]. Meanwhile, the method suggested by Fu and Kane [50] is also used to check the  $\mathbb{Z}_2$  of the centrosymmetric  $P-3m1@(\sqrt{3} \times \sqrt{3})$  structure, and consistent result is obtained. Our GGA-PBE calculations show that the  $\mathbb{Z}_2$  of all the four stable  $BC_3TI$  structures are +1, as listed in table 1, indicating that these structures are QSH insulators. Strikingly, for the  $C222@(1 \times 1)$ ,  $Pmna@(1 \times \sqrt{3})$ , and  $Pma2@(1 \times \sqrt{3})$  structures, the nonzero  $\mathbb{Z}_2$  combined with the large nontrivial gaps of 200–224 meV signifies that these structures are the 2D TIs that promise room-temperature dissipationless QSH states, similar to the functionalized germanene and stanene [13, 14].

One of the prominent features of 2D TIs is the presence of the gapless edge state with spin-momentum locking. There are two methods to get the edge state spectrum. One is to compute the band structures of the nanoribbon systems directly, and the other is to calculate the edge Green's function for a semiinfinite system [51]. We use the later method and select the (01) edge to calculate the edge state spectrum. It is worth noting that the 2D Miller index of (01) mentioned here is based on the unit cells shown in figures 2(a)–(d). The GGA-PBE calculated edge state spectra for the four stable  $BC_3TI$  structures are shown in the right panels in figure 3, in which the existence of helical Dirac edge states connecting the conduction and valence bands further indicates that these structures are indeed 2D TIs.

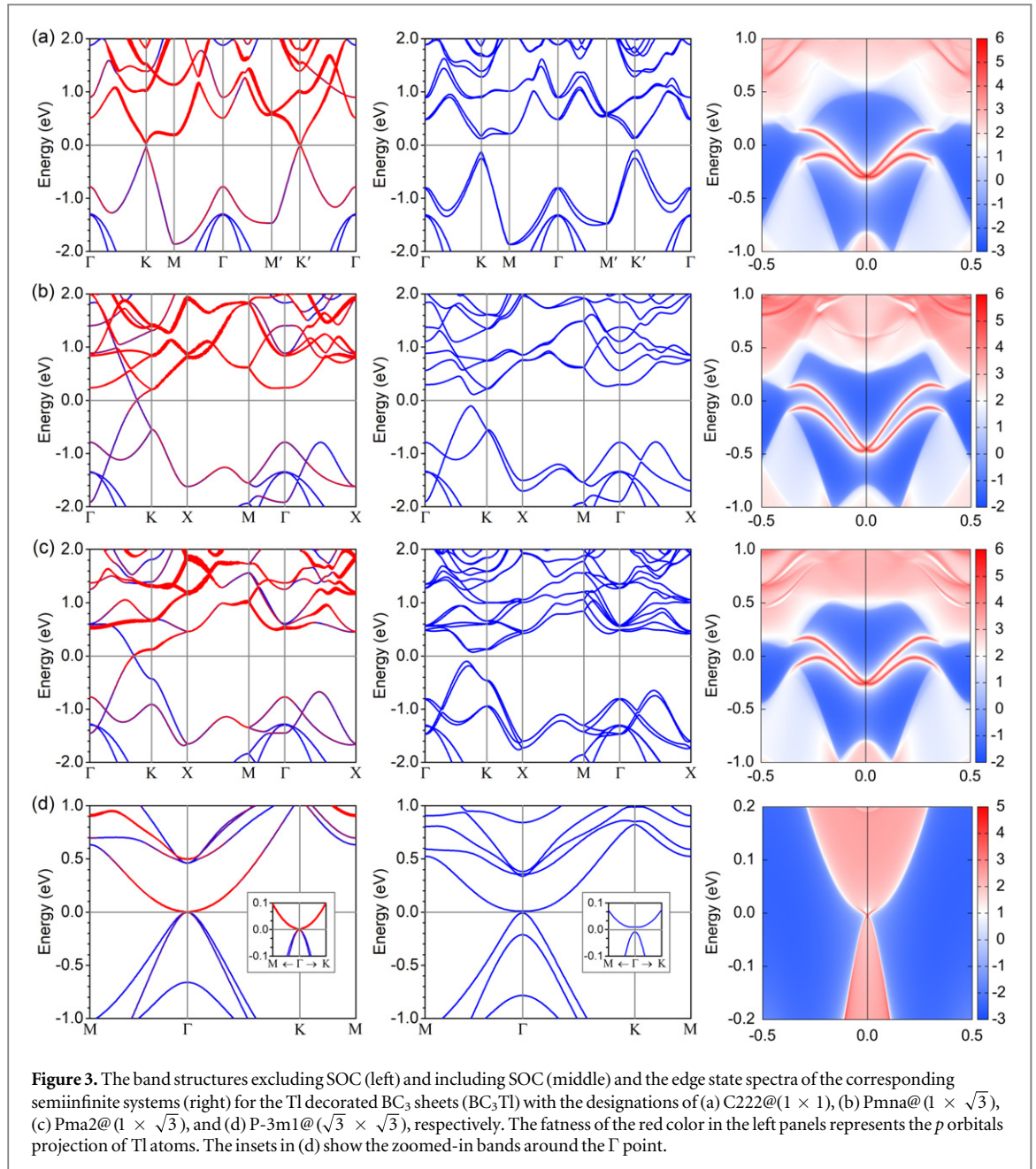


**Figure 3.** The band structures excluding SOC (left) and including SOC (middle) and the edge state spectra of the corresponding semiinfinite systems (right) for the TI decorated  $\text{BC}_3$  sheets ( $\text{BC}_3\text{TI}$ ) with the designations of (a)  $\text{C222}@ (1 \times 1)$ , (b)  $\text{Pmna}@ (1 \times \sqrt{3})$ , (c)  $\text{Pma2}@ (1 \times \sqrt{3})$ , and (d)  $\text{P-3m1}@ (\sqrt{3} \times \sqrt{3})$ , respectively. The fatness of the red color in the left panels represents the  $p$  orbitals projection of TI atoms. The insets in (d) show the zoomed-in bands around the  $\Gamma$  point.

From  $\mathbb{Z}_2$  invariants and edge states calculated by the GGA-PBE exchange-correlation functional, one can know that the topological properties of the four stable  $\text{BC}_3\text{TI}$  structures remain unchanged with the changing of adsorption configurations, which is an important feature of the topological systems. However, the topological properties are not always remaining unchanged for every stable adsorption configuration. For instance, in adatoms decorated  $(3n \times 3n)$  graphene, since Dirac cone is folded back to the  $\Gamma$  point and adatoms decoration induces a coupling between two Dirac cones, a trivial band gap around the Dirac cone is opened, and thus the topological properties of the adsorption systems are destroyed [52]. This is the so-called intervalley scattering mentioned in literatures. A typical instance for the  $\text{BC}_3$  sheet is the  $(\sqrt{3} \times \sqrt{3})$  supercell. Due to the fold of BZ, there exists a pair of Dirac cones at the  $\Gamma$  point in the bare  $(\sqrt{3} \times \sqrt{3})$   $\text{BC}_3$  sheet. After the decoration of six TI atoms, the stable  $\text{P-3m1}@ (\sqrt{3} \times \sqrt{3})$   $\text{BC}_3\text{TI}$  structure is gained, in which an accidental degeneracy between the valence and conduction bands occurs at the  $\Gamma$  point based on the GGA-PBE calculations, and the dispersion around the Dirac cone is no longer linear but become parabolic, signifying a strong intervalley scattering in this system, as shown in figure 3(d). When the SOC is included, a nontrivial gap of 20 meV is opened and thus the topological electronic properties are not destroyed by the intervalley scattering based on the GGA-PBE results. To further check the topological properties, the SCAN functional of meta-GGA [53], which is superior to most gradient corrected functionals [54], is used to recalculate the band structures and  $\mathbb{Z}_2$  invariants. The meta-GGA-SCAN calculations provide the same topological properties as those of the GGA-PBE results for the  $\text{C222}@$

**Table 2.** The calculated structural parameters (lattice vectors  $a$  and adsorption height  $h$ ), binding energies ( $E_b$ ) between adatoms and BC<sub>3</sub> sheet, cohesive energies ( $E_c$ ) of adatoms, ratios between  $E_b$  and  $E_c$  ( $E_b/E_c$ ), energy differences ( $\Delta E$ ) of ferromagnetic state relative to antiferromagnetic state, ferromagnetic moments ( $\mu$ ), energies ( $E_{MCA}$ ), nontrivial band gaps ( $E_g$ ), and Chern numbers ( $C$ ) for the  $(2 \times 2)$  BC<sub>3</sub> with one adatom of Tc, Re, or Ru and the  $(\sqrt{3} \times \sqrt{3})$  BC<sub>3</sub> with one adatom of Os.

	$a$ (Å)	$h$ (Å)	$E_b$ (eV)	$E_c$ (eV)	$E_b/E_c$	$\Delta E$ (meV)	$\mu$ ( $\mu_B$ )	$E_{MCA}$ (meV)	$E_g$ (meV)	$C$
Tc- $(2 \times 2)$ BC <sub>3</sub>	10.34	1.22	3.73	6.94	0.54	−24	1	−1.1	38	1
Re- $(2 \times 2)$ BC <sub>3</sub>	10.35	1.21	2.72	7.83	0.35	−27	1	−5.8	50	1
Ru- $(2 \times 2)$ BC <sub>3</sub>	10.35	1.32	3.67	7.03	0.52	−70	2	2.9	47	−1
Os- $(\sqrt{3} \times \sqrt{3})$ BC <sub>3</sub>	8.97	1.36	3.10	8.27	0.37	−132	2	9.8	70	−2

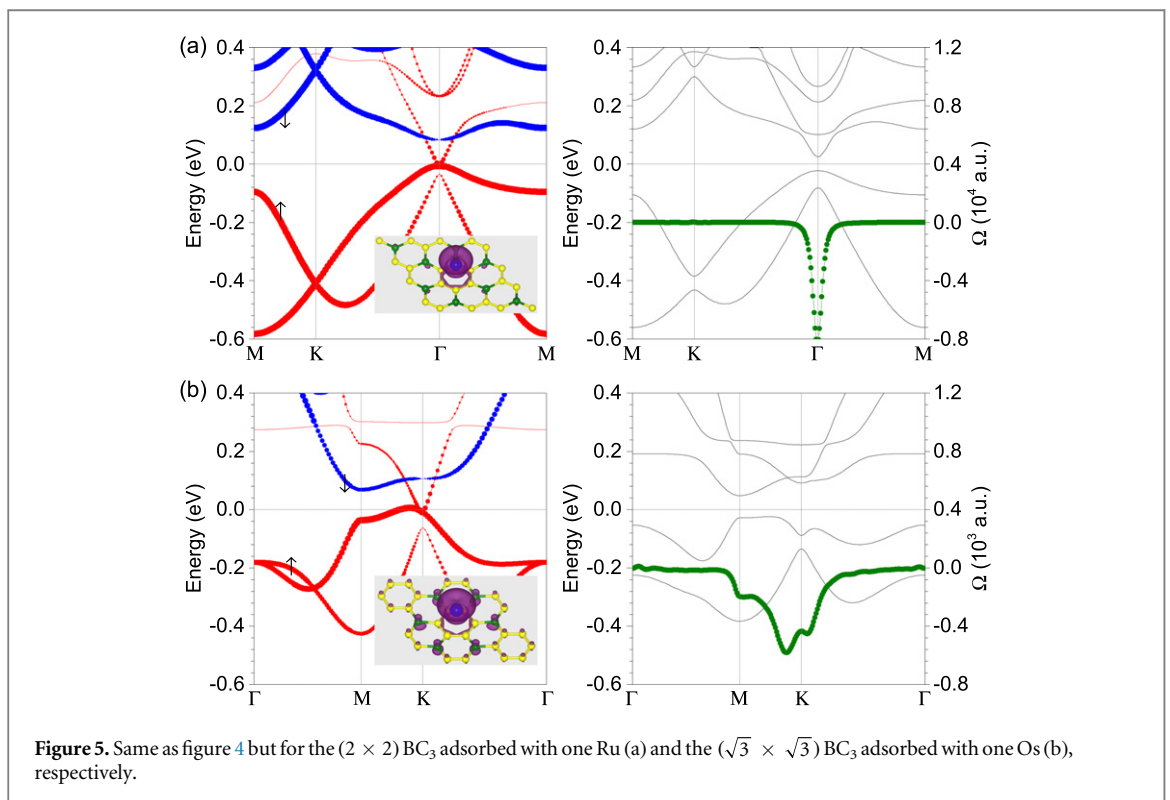
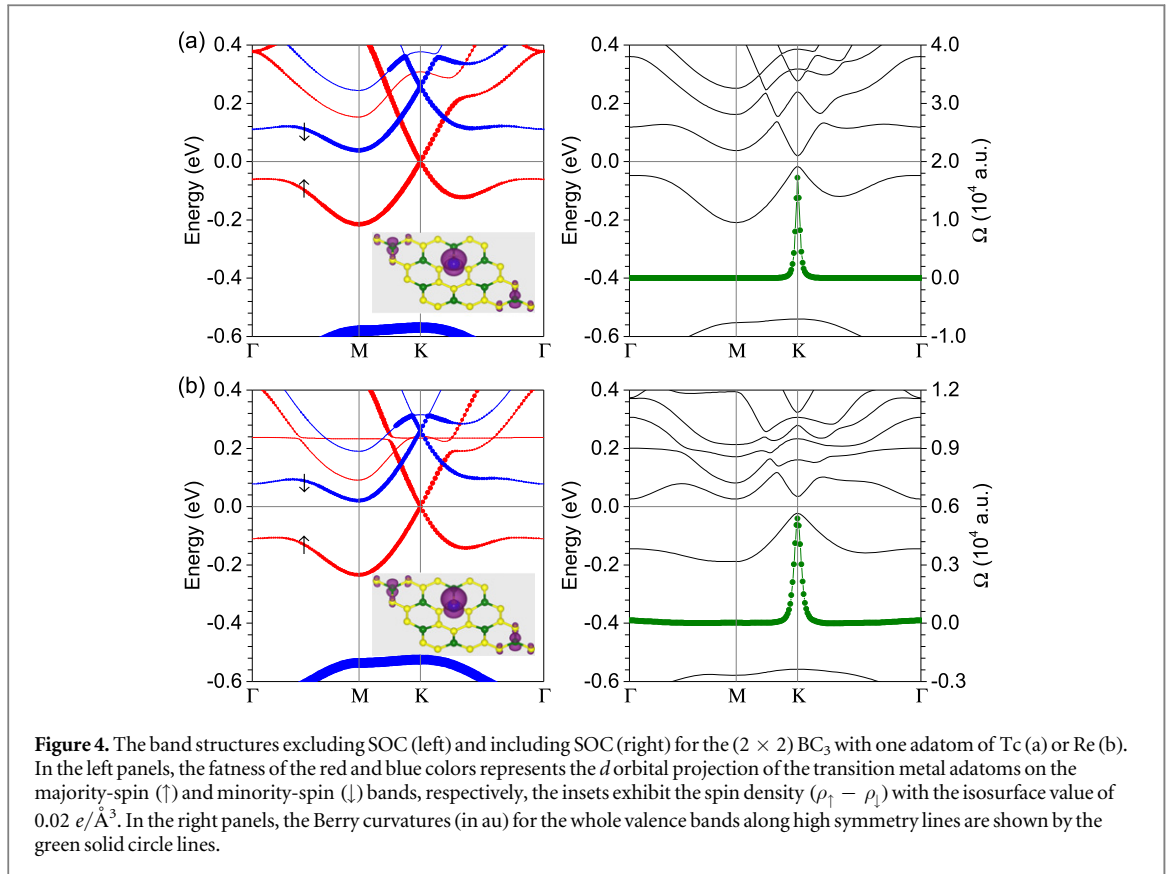
$(1 \times 1)$ , Pmna@ $(1 \times \sqrt{3})$ , and Pma2@ $(1 \times \sqrt{3})$  BC<sub>3</sub>Tl structures, as shown in figures A2(a)–(c) in the appendix. However, for the P-3m1@ $(\sqrt{3} \times \sqrt{3})$  structure, there is no degeneracy between the valence and conduction bands but a band gap of 39 meV around the Fermi level in the band structure without SOC based on the meta-GGA-SCAN calculations, as shown in figure A2(d). As a result, when the SOC is included, no band inversion occurs, the band gap only reduces to 13 meV, and consequently the calculated  $\mathbb{Z}_2$  invariant is 0, which demonstrates a destruction of the topological electronic properties by the intervalley scattering.

### 3.2. QAH states in Tc, Re, Ru, and Os adsorbed BC<sub>3</sub> sheets

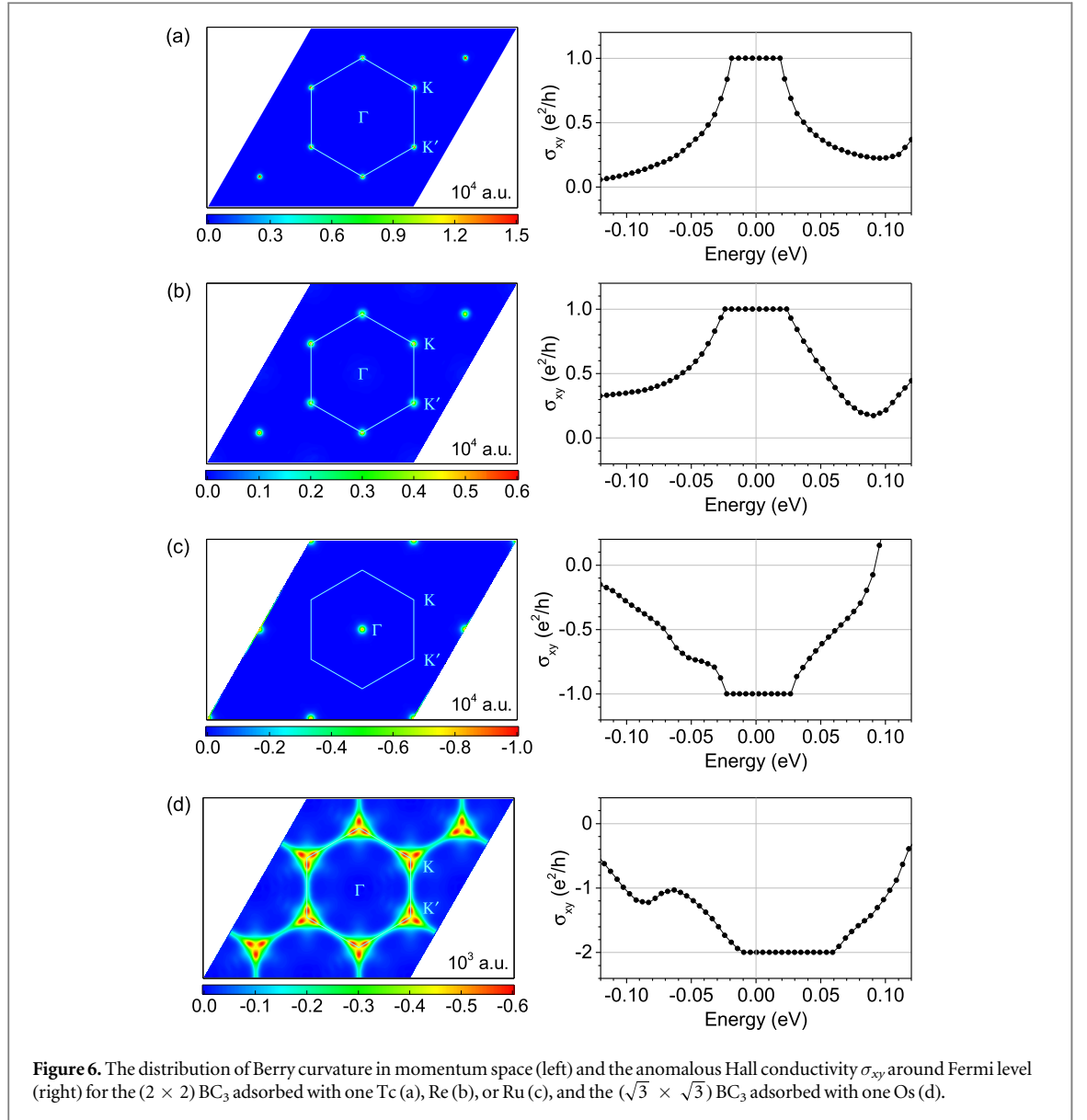
To break the TRS for seeking possible QAH state, the  $3d$ – $5d$  transition metal atoms are used to be adsorbed on BC<sub>3</sub> sheet. By traversing all of the  $3d$ – $5d$  transition metal atoms on the  $(1 \times 1)$ ,  $(\sqrt{3} \times \sqrt{3})$ , and  $(2 \times 2)$  BC<sub>3</sub> supercells, we find that the  $(2 \times 2)$  BC<sub>3</sub> with one adatom of technetium (Tc), rhenium (Re), or ruthenium (Ru) and the  $(\sqrt{3} \times \sqrt{3})$  BC<sub>3</sub> with one adatom of osmium (Os) are possible structures for realizing QAH effects. In these four adsorption structures, the transition metal adatoms are apt to be adsorbed on the hollow site of the C<sub>6</sub> rings of BC<sub>3</sub>. The structural parameters and binding energies  $E_b$  for the four structures are listed in table 2, in which the cohesive energies  $E_c$  of the bulk counterparts of adatoms are also shown. Evidently, the  $E_b$  values are smaller than those of the  $E_c$ , although they are much higher than the  $E_b$  between Tl and BC<sub>3</sub>. To verify whether the adatoms tend to cluster or not, we use a  $(4 \times 2)$  BC<sub>3</sub> to adsorb two Tc, Re, or Ru atoms and a  $(2\sqrt{3} \times \sqrt{3})$  BC<sub>3</sub> to adsorb two Os atoms on the same side. Via calculating the total energies of the adsorption configurations with different adatom–adatom distances, we find that the transition metal adatoms tend to be adsorbed on BC<sub>3</sub> discretely and thus the clustering of adatoms is effectively suppressed, which can be interpreted by the strong Coulomb repulsion between adatoms due to the electron transfer from adatoms to BC<sub>3</sub> sheet. In addition, there is no imaginary frequency in the phonon dispersion spectra of these four adsorption structures, and thus these structures locate at the local minimums in the energy landscapes, as shown in figure A3 in the appendix.

The ground states of the four stable adsorption structure are found to be ferromagnetic with the magnetic moments of  $1 \mu_B$  for the  $(2 \times 2)$  BC<sub>3</sub> with one adatom of Tc or Re and  $2 \mu_B$  for the  $(2 \times 2)$  BC<sub>3</sub> with one adatom of Ru and the  $(\sqrt{3} \times \sqrt{3})$  BC<sub>3</sub> with one adatom of Os, which are about 24–132 meV lower than their corresponding antiferromagnetic states, as listed in table 2. For the  $(2 \times 2)$  BC<sub>3</sub> with one adatom of Tc or Re, the GGA-PBE band structures excluding SOC for the ferromagnetic states are plotted in the left panels in figure 4. Owing to internal magnetization, the majority-spin (red line) and minority-spin (blue line) bands are split away from each other, and thus only the majority-spin Dirac cone bands are left around the Fermi level, giving rise to the formation of the half semimetals. Similar minority-spin Dirac cone bands are about 0.3 eV above the Fermi level. The spin densities ( $\rho_\uparrow - \rho_\downarrow$ ) shown in the insets exhibit that the ferromagnetic moments are mainly distributed around the adatoms. The atomic orbital projections on the bands demonstrate that a large part of the Dirac cone states around the Fermi level are contributed by the  $d$  orbital electrons of the adatoms, implying strong SOC in these adsorption systems. Therefore, when the SOC is included, the large nontrivial band gap of about 38 (58) meV is opened at the K point for the  $(2 \times 2)$  BC<sub>3</sub> with one adatom of Tc (Re), as shown in the right panels in figure 4. In addition, for the  $(2 \times 2)$  BC<sub>3</sub> adsorbed with one Re, due to the drastic up-move of conduction band at the K point, the conduction band minimum shifts to the M point, which results in an indirect band gap of about 50 meV in this system, as shown in the right panel in figure 4(b).

The GGA-PBE band structures excluding SOC and including SOC for the  $(2 \times 2)$  BC<sub>3</sub> with one adatom of Ru and the  $(\sqrt{3} \times \sqrt{3})$  BC<sub>3</sub> with one adatom of Os are plotted in figures 5(a) and (b), respectively. Different from the bands of the  $(2 \times 2)$  BC<sub>3</sub> adsorbed with one Tc or Re, the Dirac cone states at the K point in the band excluding SOC for the  $(2 \times 2)$  BC<sub>3</sub> with one adatom of Ru are far away from Fermi level. However, a majority-spin semimetal state at the  $\Gamma$  point is present around the Fermi level, which is mainly provided by the  $d$  orbital electrons of the Ru adatom. Thus, when the SOC is included, a nontrivial band gap of about 47 meV is opened in this system, as shown in the right panel in figure 5(a). For the  $(\sqrt{3} \times \sqrt{3})$  BC<sub>3</sub> adsorbed with one Os, a majority-spin degeneracy point exists at the K point nearby 7 meV below Fermi level in the band excluding SOC based on



the GGA-PBE results. Meanwhile, the valence band along the MK line and the conduction band around the K point are both crossed some by Fermi level, which makes the system be an ordinary halfmetal. Fortunately, because of the strong SOC of Os adatom, the band structure including SOC gives an insulating state with the conduction band minimum at the M point, the valence band maximum at the middle point of the MK line, and a nontrivial gap of about 70 meV, as shown in the right panel in figure 5(b).



To identify the topological properties of the SOC induced insulating states, we calculate the Berry curvatures and Chern numbers for the four stable adsorption structures. The Berry curvatures  $\Omega(\mathbf{k})$  are calculated using the Kubo formula [55, 56]

$$\Omega(\mathbf{k}) = \sum_n f_n \Omega_n(\mathbf{k}),$$

$$\Omega_n(\mathbf{k}) = - \sum_{m \neq n} 2 \operatorname{Im} \frac{\langle \psi_{n\mathbf{k}} | v_x | \psi_{m\mathbf{k}} \rangle \langle \psi_{m\mathbf{k}} | v_y | \psi_{n\mathbf{k}} \rangle}{(\varepsilon_{m\mathbf{k}} - \varepsilon_{n\mathbf{k}})^2}, \quad (1)$$

where the summation is over all occupied states,  $\varepsilon_{n\mathbf{k}}$  and  $\psi_{n\mathbf{k}}$  are the eigenvalue and Bloch function of band  $n$  at wave vector  $\mathbf{k}$ ,  $f_n$  is the Fermi–Dirac distribution function of band  $n$ , and  $v_x$  and  $v_y$  are the velocity operators. Through the gauge transfer between Bloch functions and real space Wannier functions, the Berry curvatures  $\Omega(\mathbf{k})$  are computed directly from the formula (32) of [57]. Via integration of the  $\Omega(\mathbf{k})$  over the first BZ, the Chern numbers ( $C$ ) and anomalous Hall conductivities ( $\sigma_{xy}$ ) are calculated by the formulas  $C = \frac{1}{2\pi} \int_{\text{BZ}} d^2k \Omega$  and  $\sigma_{xy} = \frac{e^2}{h} C$ .

The GGA-PBE results of Berry curvatures  $\Omega(\mathbf{k})$  (in au) for the whole valence bands along high symmetry lines for the  $(2 \times 2)$  BC<sub>3</sub> with one adatom of Tc, Re, or Ru and the  $(\sqrt{3} \times \sqrt{3})$  BC<sub>3</sub> with one adatom of Os are plotted by the green solid circle lines in figures 4 and 5, which exhibits that the most nonzero Berry curvatures  $\Omega(\mathbf{k})$  only occur nearby the SOC induced nontrivial gaps. The corresponding distributions of the  $\Omega(\mathbf{k})$  in the momentum spaces are shown in the left panels in figure 6. For the  $(2 \times 2)$  BC<sub>3</sub> adsorbed with one Tc or Re, the nonzero  $\Omega(\mathbf{k})$  are localized around the K and K' points with the same sign, while the nonzero  $\Omega(\mathbf{k})$  for the  $(2 \times 2)$  BC<sub>3</sub> adsorbed with one Ru are located around the  $\Gamma$  point, as shown in the left panels in figures 6(a)–(c). For the  $(\sqrt{3} \times \sqrt{3})$  BC<sub>3</sub> adsorbed with one Os, there exists

conspicuous distribution of  $\Omega(\mathbf{k})$  around the whole  $KK'$  line with the maximum value nearby the K and  $K'$  points based on the GGA-PBE calculations, as shown in the left panel in figure 6(d). By integrating the  $\Omega(\mathbf{k})$  over the first BZ, the anomalous Hall conductivities  $\sigma_{xy}$ , as a function of the energy around the Fermi level are obtained for the four adsorption structures, as shown in the right panels in figure 6. One can find that the quantized Hall conductance platforms appear around the Fermi level and the widths of the platforms for the four adsorption structures accord completely with their global band gaps obtained from the GGA-PBE first-principles calculations. The Chern number of all occupied bands for the  $(2 \times 2)$   $BC_3$  with one adatom of Tc or Re is the integer value of 1, and the Chern numbers for the  $(2 \times 2)$   $BC_3$  with one adatom of Ru and the  $(\sqrt{3} \times \sqrt{3})$   $BC_3$  with one adatom of Os are  $-1$  and  $-2$ , respectively, as listed in table 2. These nonzero Chern numbers indicate that the four adsorption structures are topologically nontrivial and thus two chiral edge channels appear on each side of their samples. In addition, for further verification of the topological properties, the SCAN functional of meta-GGA is also used to recalculate the band structures and Chern numbers of the four adsorption structures. The meta-GGA-SCAN calculations provide the same topological properties as those of the GGA-PBE results for the three adsorption structures of the  $(2 \times 2)$   $BC_3$  with one adatom of Tc, Re, or Ru, as shown in figures A4(a)–(c) in the appendix. But, for the  $(\sqrt{3} \times \sqrt{3})$   $BC_3$  with one adatom of Os, the band structure excluding SOC have a band gap of 268 meV around the Fermi level based on the meta-GGA-SCAN results, which is in sharp contrast to the halfmetal state obtained from the GGA-PBE calculations, as shown in figure A4(d). Thus, when the SOC is included, there is no band inversion occurring, the band gap only becomes 172 meV, and consequently the calculated Chern number is 0, which can also be explained by the strong intervalley scattering in the  $(\sqrt{3} \times \sqrt{3})$   $BC_3$  supercell. These results means that the realization of the robust QAH effects are only feasible in the systems of the  $(2 \times 2)$   $BC_3$  with one adatom of Tc, Re, or Ru.

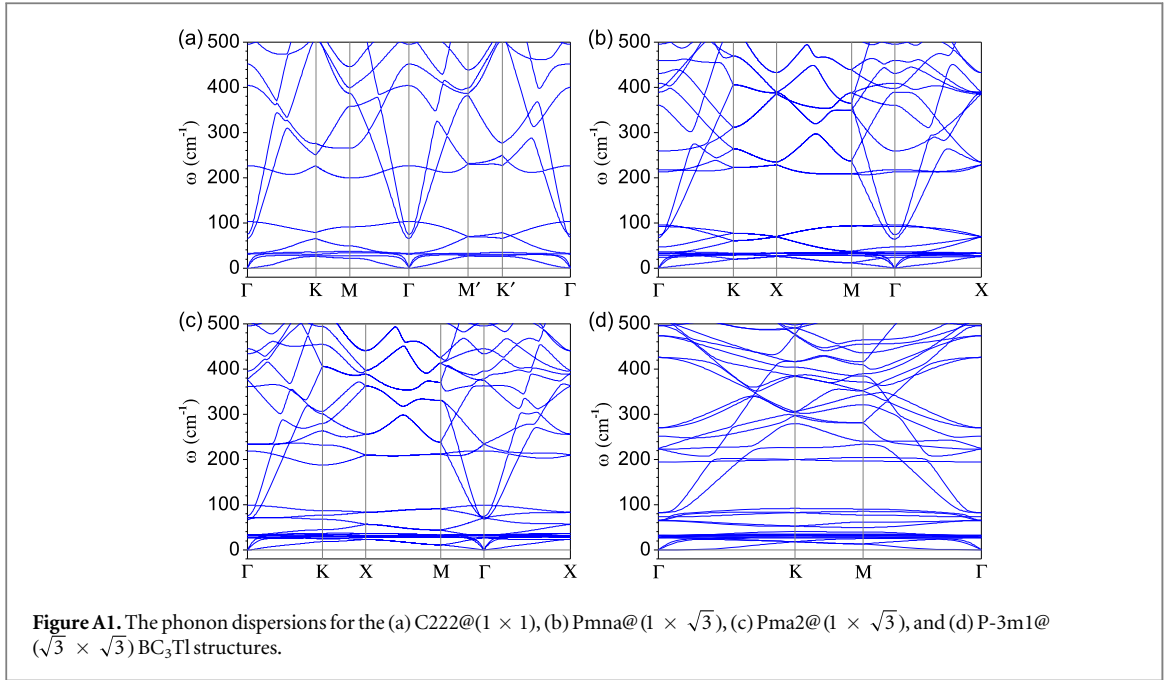
In order to confirm the easy magnetization orientation, we also calculate the magnetocrystalline anisotropy of the four adsorption structures, which is the total energy difference between two magnetic states where the magnetization is aligned along the [100] or [001] direction, i.e.,  $E_{MCA} = E_{[100]} - E_{[001]}$ . Our calculations indicate that the energy of the out-of-plane spin orientation for the  $(2 \times 2)$   $BC_3$  adsorbed with one Tc or Re is about 1.1 or 5.8 meV lower than that of the in-plane spin orientation, while the adsorbed states of the  $(2 \times 2)$   $BC_3$  with one Ru adatom and the  $(\sqrt{3} \times \sqrt{3})$   $BC_3$  with one Os adatom have the in-plane spin orientations, as listed in table 2. Thus, the  $(2 \times 2)$   $BC_3$  adsorbed with one Tc or Re are the suitable systems to observe the QAH states in experiments. Furthermore, due to the existence of the largest ratio of  $E_b/E_c$  in the four adsorption structures, the  $(2 \times 2)$   $BC_3$  adsorbed with one Tc is the best system to realize the QAH effect. In addition, it is known that the QAH effects can be effectively manipulated through changing of the easy magnetization axis by external electric fields [22]. For the  $(2 \times 2)$   $BC_3$  adsorbed with one Ru, a suitable external electric field is suggested to tune the QAH effects for possible experimental observation.

## 4. Conclusion

In summary, we have used first-principles calculations combined with Wannier functions-based TB modeling to compute the topological electronic properties of graphenelike  $BC_3$  based systems. We discover that the Tl decorated  $BC_3$  systems with the same stoichiometry of  $BC_3Tl$  have three low-energy structures that are confirmed to be robust 2D TIs with the nontrivial band gaps exceeding 200 meV, which promises room-temperature dissipationless QSH states. In addition, these topological  $BC_3Tl$  structures are verified by the *ab initio* evolutionary algorithm to be more stable than other 2D  $BC_3Tl$  allotropes, implying that these structures may be synthesized directly on a suitable substrate in an epitaxial way. By traversing all of the  $3d$ – $5d$  transition metal atoms on different  $BC_3$  supercells, we reveal that the  $(2 \times 2)$   $BC_3$  adsorbed with one Tc, Re, or Ru are robust CIs with ferromagnetic ground states, nontrivial band gaps larger than 38 meV, and nonzero Chern numbers. The  $(2 \times 2)$   $BC_3$  adsorbed with one adatom Tc or Re are the suitable systems for observing the QAH effects experimentally because in these systems the energy of the out-of-plane spin orientation is lower than that of the in-plane spin orientation. For the  $(2 \times 2)$   $BC_3$  adsorbed with one Ru, a suitable external electric field is suggested for possible experimental observation. These results demonstrate that the systems of graphenelike  $BC_3$  with suitable decoration of adatoms are good platforms for realizing QSH and QAH states.

## Acknowledgments

This research was supported by the Natural Science Foundation of Shandong Province for Doctoral Program under Grant No. ZR2017BA017, the National Natural Science Foundation of China under Grant Nos. 11704322, 11774396, and 11774195, and the National Key Research and Development Program of China under Grant Nos. 2016YFA0300902 and 2016YFB0700102.



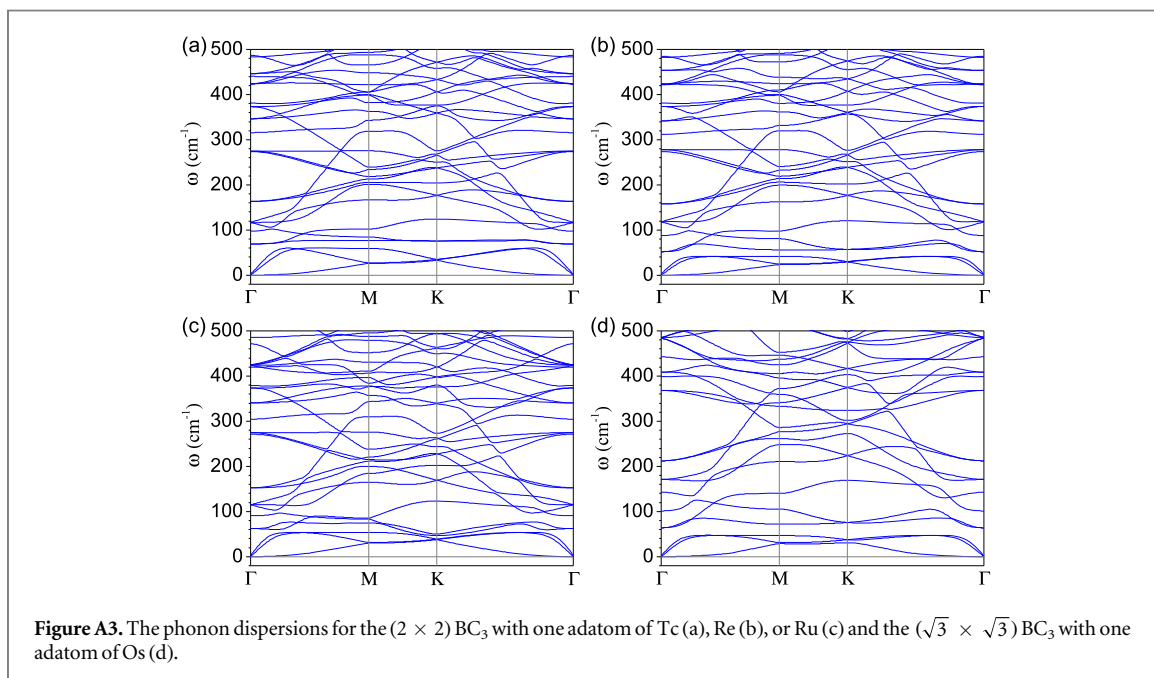
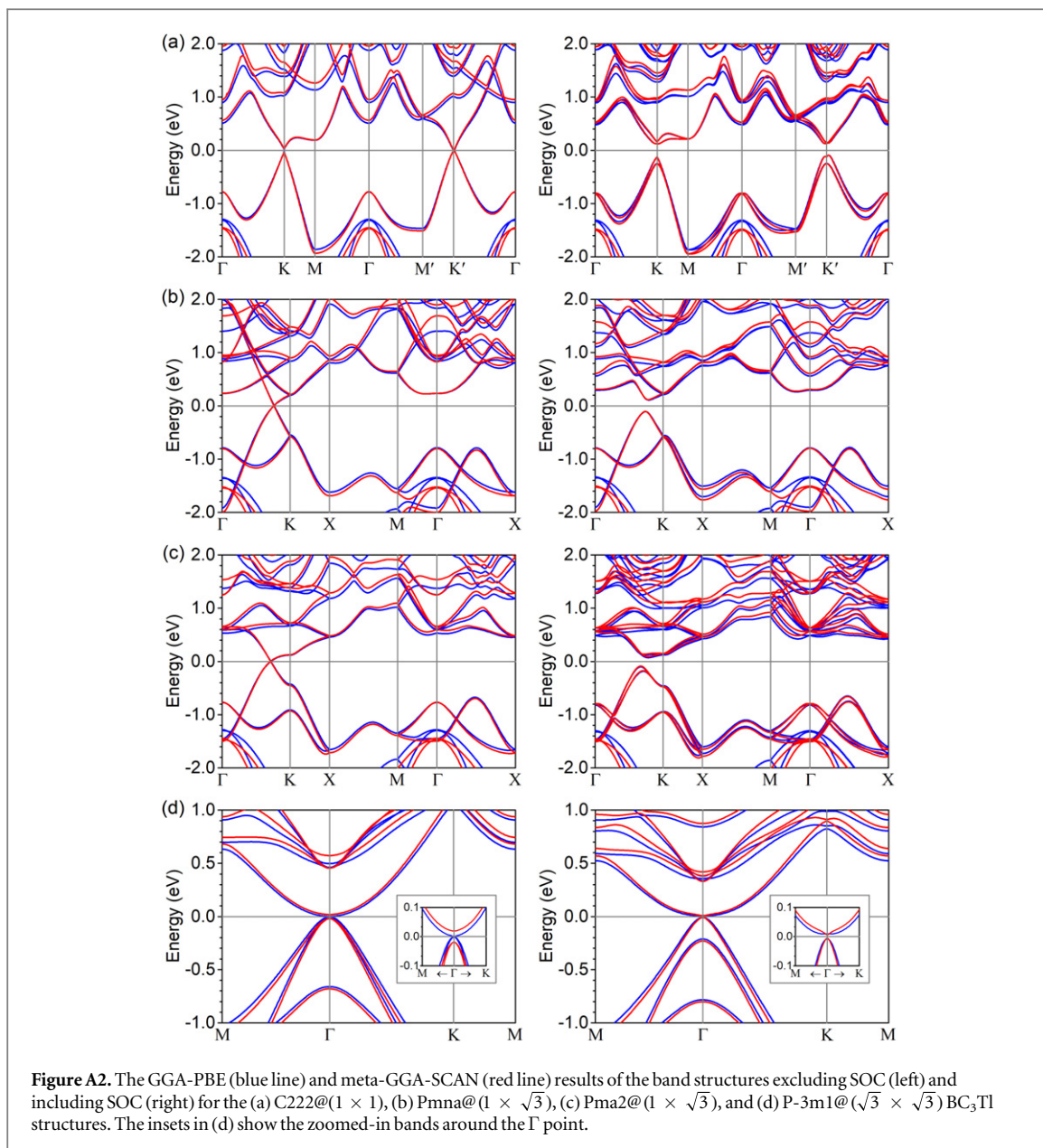
## Appendix

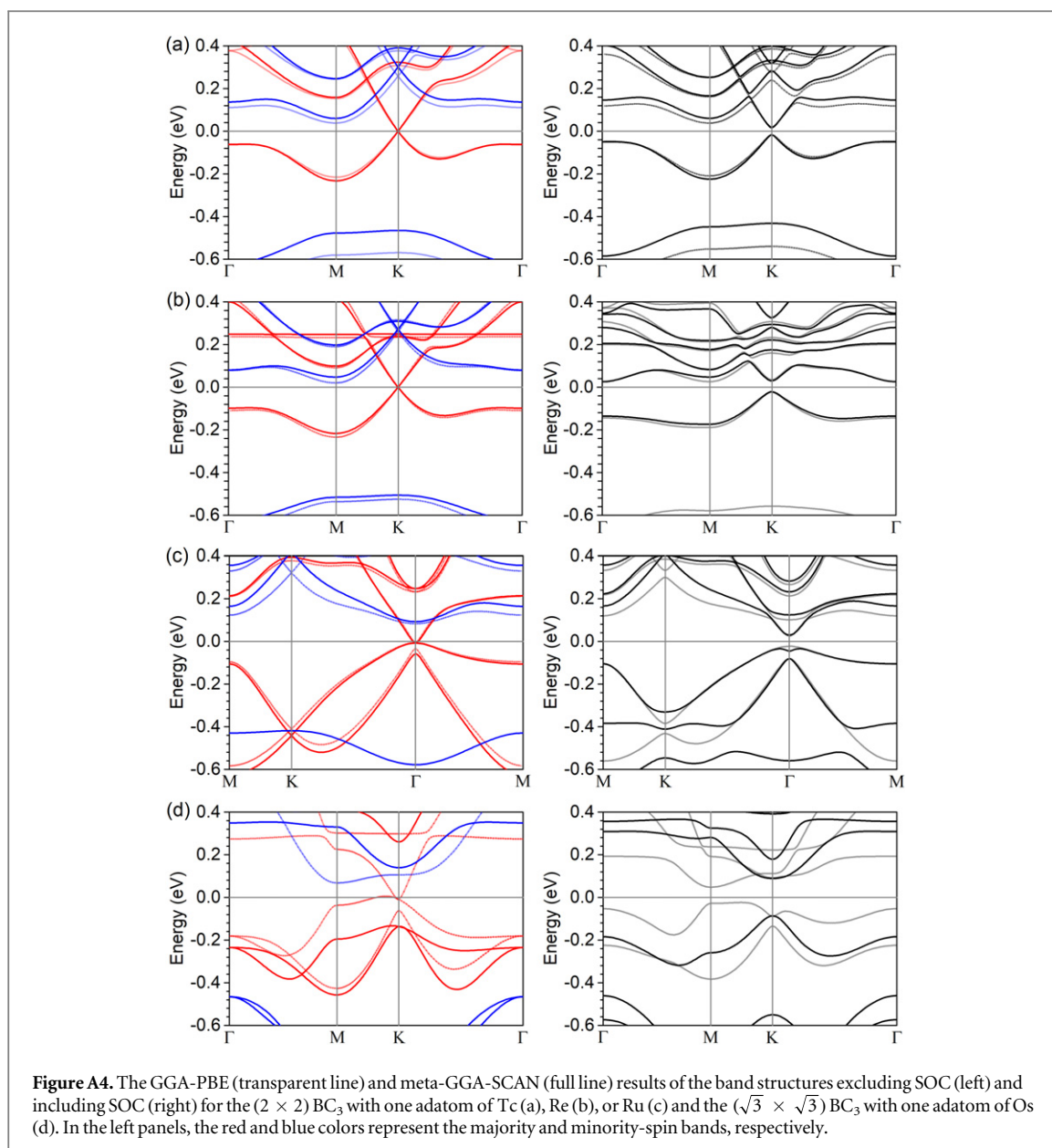
To check the local stabilities of the four low-energy BC<sub>3</sub>Tl allotropes shown in figures 2(a)–(d), we calculate their phonon dispersion relations via the finite-difference approach. The required harmonic interatomic force constants for the C222@(1 × 1), Pmna@(1 × √3), Pma2@(1 × √3), and P-3m1@(√3 × √3) BC<sub>3</sub>Tl structures are generated within the (3 × 3), (3 × 2), (3 × 2), and (2 × 2) supercells with respect to their unit cells. The calculated phonon spectra are plotted in figure A1, in which the absence of imaginary frequency demonstrates the local stability, hinting that all of these four structures locate their local minimums in the energy landscapes.

The meta-GGA-SCAN results of the band structures excluding and including SOC for the C222@(1 × 1), Pmna@(1 × √3), Pma2@(1 × √3), and P-3m1@(√3 × √3) BC<sub>3</sub>Tl structures are plotted in figure A2. For comparison, the GGA-PBE results are also plotted. For the C222@(1 × 1), Pmna@(1 × √3), and Pma2@(1 × √3) structures, the meta-GGA-SCAN calculations have no essential difference with the GGA-PBE results, and the SOC induced gaps opened are almost unchanged, as shown in figures A2(a)–(c). Meanwhile, the calculated  $\mathbb{Z}_2$  invariants via the meta-GGA-SCAN functional for the three structures are all +1, same as the GGA-PBE results. However, for the P-3m1@(√3 × √3) structure, there is a band gap of about 39 meV around the Fermi level in the band structure excluding SOC based on the GGA-PBE calculations, which is in contrast to the accidental degeneracy induced semimetal state obtained from the GGA-PBE calculations, as shown in the insets in figure A2(d). When the SOC is included, the band gap only reduces to about 13 meV, and no band inversion occurs. As a result, the calculated  $\mathbb{Z}_2$  invariants from the meta-GGA-SCAN functional for this structure is 0, which is interpreted by the strong intervalley scattering that can destroy the topological properties of the adsorption systems within (3n × 3n) and (√3n × √3n) supercells [52].

In order to verify the local stabilities of the (2 × 2) BC<sub>3</sub> adsorbed with one Tc, Re, or Ru and the (√3 × √3) BC<sub>3</sub> adsorbed with one Os, we also calculate corresponding phonon dispersion relations. The required harmonic interatomic force constants for the four adsorption systems are all generated within the (2 × 2) supercells relative to their unit cells, that is, the supercells with the (4 × 4) and (2√3 × 2√3) BC<sub>3</sub>. The calculated phonon spectra are plotted in figure A3, in which the absence of imaginary frequency verifies the local stability.

The meta-GGA-SCAN results of the band structures excluding and including SOC for the (2 × 2) BC<sub>3</sub> with one adatom of Tc, Re, or Ru and the (√3 × √3) BC<sub>3</sub> with one adatom of Os are plotted in figure A4. The GGA-PBE results are also plotted for comparison. For the three structures of the (2 × 2) BC<sub>3</sub> with one adatom of Tc, Re, or Ru, the meta-GGA-SCAN calculations indicate similar band structures to the GGA-PBE results, as shown in figures A4(a)–(c). At the same time, the calculated Chern numbers by the meta-GGA-SCAN functional are also same as the GGA-PBE calculations. But, for the (√3 × √3) BC<sub>3</sub> adsorbed with one Os, a band gap of about 268 meV around the Fermi level is obtained in the band structure excluding SOC based on the GGA-PBE calculations, in sharp contrast to the halfmetal state obtained from the GGA-PBE calculations, as shown in the insets in figure A4(d). When the SOC is included, the band gap only reduces to 172 meV, and no band inversion





occurs. Thus, the calculated Chern number becomes 0, which can be also explained by the strong intervalley scattering in the  $(\sqrt{3} \times \sqrt{3})$   $\text{BC}_3$  supercell.

## ORCID iDs

Zhenhong Dai  <https://orcid.org/0000-0002-8559-3196>

Chao Zhang  <https://orcid.org/0000-0002-5957-2287>

## References

- [1] Nagaosa N 2007 *Science* **318** 758
- [2] Hasan M Z and Kane C L 2010 *Rev. Mod. Phys.* **82** 3045
- [3] Qi X-L and Zhang S-C 2011 *Rev. Mod. Phys.* **83** 1057
- [4] Hsieh D et al 2009 *Nature* **460** 1101
- [5] Moore J 2009 *Nat. Phys.* **5** 378
- [6] Fu L, Kane C L and Mele E J 2007 *Phys. Rev. Lett.* **98** 106803
- [7] Rasche B, Isaeva A, Ruck M, Borisenko S, Zabolotnyy V, Büchner B, Koepfner K, Ortix C, Richter M and van den Brink J 2013 *Nat. Mater.* **12** 422
- [8] Hsieh D et al 2009 *Phys. Rev. Lett.* **103** 146401
- [9] Chen Y L et al 2009 *Science* **325** 178
- [10] Bernevig B A, Hughes T L and Zhang S-C 2006 *Science* **314** 1757

- [11] König M, Wiedmann S, Brüne C, Roth A, Buhmann H, Molenkamp L W, Qi X-L and Zhang S-C 2007 *Science* **318** 766
- [12] Knez I, Du R-R and Sullivan G 2011 *Phys. Rev. Lett.* **107** 136603
- [13] Xu Y, Yan B, Zhang H-J, Wang J, Xu G, Tang P, Duan W and Zhang S-C 2013 *Phys. Rev. Lett.* **111** 136804
- [14] Si C, Liu J, Xu Y, Wu J, Gu B-L and Duan W 2014 *Phys. Rev. B* **89** 115429
- [15] Liu C-C, Guan S, Song Z, Yang S A, Yang J and Yao Y 2014 *Phys. Rev. B* **90** 085431
- [16] Ma Y, Kou L, Li X, Dai Y and Heine T 2016 *Phys. Rev. B* **93** 035442
- [17] Ma Y, Kou L, Dai Y and Heine T 2016 *Phys. Rev. B* **94** 201104
- [18] Ma Y, Kou L, Li X, Dai Y and Heine T 2016 *NPG Asia Mater.* **8** e264
- [19] Haldane F D M 1988 *Phys. Rev. Lett.* **61** 2015
- [20] Liu C-X, Qi X-L, Dai X, Fang Z and Zhang S-C 2008 *Phys. Rev. Lett.* **101** 146802
- [21] Yu R, Zhang W, Zhang H-J, Zhang S-C, Dai X and Fang Z 2010 *Science* **329** 61
- [22] Zhang H, Lazo C, Blügel S, Heinze S and Mokrousov Y 2012 *Phys. Rev. Lett.* **108** 056802
- [23] Wang Z F, Liu Z and Liu F 2013 *Phys. Rev. Lett.* **110** 196801
- [24] Garrity K F and Vanderbilt D 2013 *Phys. Rev. Lett.* **110** 116802
- [25] Zhang H, Wang J, Xu G, Xu Y and Zhang S-C 2014 *Phys. Rev. Lett.* **112** 096804
- [26] Cai T, Li X, Wang F, Ju S, Feng J and Gong C-D 2015 *Nano Lett.* **15** 6434
- [27] Chang C-Z et al 2013 *Science* **340** 167
- [28] Qiao Z, Yang S A, Feng W, Tse W-K, Ding J, Yao Y, Wang J and Niu Q 2010 *Phys. Rev. B* **82** 161414
- [29] Zhang J, Zhao B and Yang Z 2013 *Phys. Rev. B* **88** 165422
- [30] Ding J, Qiao Z, Feng W, Yao Y and Niu Q 2011 *Phys. Rev. B* **84** 195444
- [31] Yanagisawa H, Tanaka T, Ishida Y, Matsue M, Rokuta E, Otani S and Oshima C 2004 *Phys. Rev. Lett.* **93** 177003
- [32] Yang Z and Ni J 2010 *Appl. Phys. Lett.* **97** 253117
- [33] Yang Z and Ni J 2012 *Appl. Phys. Lett.* **100** 183109
- [34] Chen X and Ni J 2013 *Phys. Rev. B* **88** 115430
- [35] Kouvetakis J, Kaner R B, Sattler M L and Bartlett N 1986 *J. Chem. Soc. Chem. Commun.* **0** 1758
- [36] Novoselov K S, Jiang D, Schedin F, Booth T J, Khotkevich V V, Morozov S V and Geim A K 2005 *Proc. Natl Acad. Sci. USA* **102** 10451
- [37] Chen X, Yao Y, Yao H, Yang F and Ni J 2015 *Phys. Rev. B* **92** 174503
- [38] Kresse G and Furthmüller J 1996 *Phys. Rev. B* **54** 11169
- [39] Kresse G and Furthmüller J 1996 *Comput. Mater. Sci.* **6** 15
- [40] Kresse G and Joubert D 1999 *Phys. Rev. B* **59** 1758
- [41] Perdew J P, Burke K and Ernzerhof M 1996 *Phys. Rev. Lett.* **77** 3865
- [42] Mostofi A A, Yates J R, Lee Y-S, Souza I, Vanderbilt D and Marzari N 2008 *Comput. Phys. Commun.* **178** 685
- [43] Wu Q, Zhang S, Song H-F, Troyer M and Soluyanov A A 2018 *Comput. Phys. Commun.* **224** 405
- [44] Gresch D, Autès G, Yazyev O V, Troyer M, Vanderbilt D, Bernevig B A and Soluyanov A A 2017 *Phys. Rev. B* **95** 075146
- [45] Oganov A R and Glass C W 2006 *J. Chem. Phys.* **124** 244704
- [46] Glass C W, Oganov A R and Hansen N 2006 *Comput. Phys. Commun.* **175** 713
- [47] Zhu Q, Li L, Oganov A R and Allen P B 2013 *Phys. Rev. B* **87** 195317
- [48] Yu R, Qi X L, Bernevig A, Fang Z and Dai X 2011 *Phys. Rev. B* **84** 075119
- [49] Soluyanov A A and Vanderbilt D 2011 *Phys. Rev. B* **83** 235401
- [50] Fu L and Kane C L 2007 *Phys. Rev. B* **76** 045302
- [51] Sancho M P L, Sancho J M L, Sancho J M L and Rubio J 1985 *J. Phys. F: Met. Phys.* **15** 851
- [52] Jiang H, Qiao Z, Liu H, Shi J and Niu Q 2012 *Phys. Rev. Lett.* **109** 116803
- [53] Sun J, Ruzsinszky A and Perdew J P 2015 *Phys. Rev. Lett.* **115** 036402
- [54] Sun J et al 2016 *Nat. Chem.* **8** 831
- [55] Thouless D J, Kohmoto M, Nightingale M P and den Nijs M 1982 *Phys. Rev. Lett.* **49** 405
- [56] Yao Y, Kleinman L, MacDonald A H, Sinova J, Jungwirth T, Wang D-S, Wang L and Niu Q 2004 *Phys. Rev. Lett.* **92** 037204
- [57] Wang X, Yates J R, Souza I and Vanderbilt D 2006 *Phys. Rev. B* **74** 195118